Stokes drift and wind drift in a rotating equilibrium sea

R. M. Samelson and S. F. Zippel

College of Earth, Ocean, and Atmospheric Sciences, Oregon State University
Corvallis, OR 97331-5503, USA

22 Aug 2025

Corresponding author: R. M. Samelson, roger.samelson@oregonstate.edu

ABSTRACT: Stokes drift may be regarded as the wave-correlated mean component of horizontal fluid motion in a surface gravity wave field. For linear, sinusoidal, non-rotating waves, this wave drift can be computed kinematically using Lagrangian, fixed-depth (relative to the mean sea surface) Eulerian, or surface-conforming Eulerian means. To understand the corresponding motion that is induced in the rotating frame in an equilibrium wind-sea, it is necessary to consider the forced-damped momentum balance that maintains the drift. It is natural to associate the force with the wave-correlated pressure force on the free surface, which imparts momentum but no vorticity to the wave field. The damping presumably derives primarily from wave-breaking, for which an idealized representation is introduced in terms of linear drag with a damping timescale derived from equilibrium wind-wave theory. The resulting forced-damped wave and mean wave-drift momentum balances are examined, for both Eulerian mean representations of the mean momentum balances. It is concluded that in a rotating equilibrium sea with Coriolis parameter computed at 40° N, the mean Stokes drift will be directed up to $10° - 45°$ to the right of downwind, depending on depth, wavelength, and wind-wave amplitude or wind speed. The parameterized wave-breaking force and the wave drift for a rotating equilibrium-sea spectral wave field are combined with a recently-proposed, semi-empirical, rotating equilibrium-sea wind-drift model to obtain predictions of the combined wind and wave drift. The resulting predictions differ modestly but systematically from wind-drift-only predictions from the rotating equilibrium-sea wind-drift model.

1. Introduction

When the wind blows over the sea surface, the transfer of momentum across the air-sea interface induces and is supported by a combination of surface wave and near-surface turbulent, wave-coherent and mean motions. Even for uniform density, incompressible fluids, the resulting problem for the detailed dynamics of the full turbulent and wave motion is beyond present theoretical understanding (see, e.g., Phillips 1977; Sullivan and McWilliams 2010; D'Asaro et al. 2014; Sutherland and Melville 2015; Grare et al. 2018; Pizzo et al. 2021, and numerous related works). Simple theoretical ideas, beginning with the classical, constant turbulent viscosity model of Ekman (1905), have nonetheless proven useful for the conceptual and, in part, quantitative description of the mean wind-driven motion in the surface ocean boundary layer, as demonstrated for example by the observational analysis of Chereskin (1995). It is generally accepted, however, that the wind-driven motion in the upper few meters departs significantly from that predicted by the classical Ekman model with constant turbulent viscosity (e.g., Ardhuin et al. 2009; Rascle and Ardhuin 2009; Zelenke et al. 2012; Morey et al. 2018; Laxague and Zappa 2020). This near-surface "wind-drift" component of the mean wind-driven motion tends to have a greater downwind component and larger magnitude than the near-surface velocity predicted by the Ekman (1905) constant turbulent viscosity model but a broadly accepted, quantitative, physical model of this mean near-surface wind drift does not presently exist.

A simple but novel semi-empirical model of the near-surface wind drift under the statistically stationary conditions of a homogeneous, equilibrium sea was proposed recently by Samelson (2022). The new elements of this model included a wind-speed-dependent roughness length, a wind-speed-dependent wave correction factor, and a mass-weighted, surface-conforming, spatial-average Eulerian mean velocity. The parameterized roughness length and wave correction factor allowed large departures of the wave-affected near-surface conditions from those represented by standard values of the roughness length and von Kàrmàn constant for rigid-surface wall boundary layers. The surface-conforming Eulerian mean was shown to capture the mean wave-drift momentum of linear surface gravity waves that in the Lagrangian representation is generally known as Stokes drift and which is generally missed by traditional, fixed-depth Eulerian means. This wind-drift model has been compared with an extensive, multi-instrument, in-situ and remote-sensing dataset of near-surface velocity measurements from the Sub-Mesoscale Ocean Dynamics Experiment (Farrar et al. 2025) and shown to have useful skill for the range of conditions represented in the dataset (Leyba et al. In preparation). The best results in that comparison were obtained for modified versions of the roughness length and wave-correction factor parameterizations originally proposed by Samelson (2022).

A limitation of the Samelson (2022) model is that while the mean horizontal velocity was formulated to capture the mean Stokes drift from the equilibrium-sea wave field, the downward momentum transport was modeled as an effective turbulent stress and did not incorporate a body force component that might be anticipated to offer a more physically consistent representation of any mean wave-coherent pressure forcing that may be associated with the surface wave field. The main goal of the work described here is to explore this possibility by constructing a simple physical model of forced-damped wave drift in a rotating ocean, and then combining the wave-drift model and the implied wave-coherent body forcing with the Samelson (2022) wind-drift model to obtain a model of the total equilibrium-sea wind and wave drift. The resulting considerations lead also to the conclusion that, under equilibrium-sea conditions in a rotating ocean, a wavelength-dependent rotation of the mean Stokes drift arises that is analogous to the depth-dependent rotation of the classical Ekman (1905) mean wind drift. Essentially, the damping modifies the inviscid rotating wave balance such that the induced inertial oscillations described by Hasselmann (1970) are replaced by rotation of the mean forced-damped wave drift.

2. Wave drift for linear rotating waves

a. Linear equations with rotation and damping

In the equilibrium-sea setting, it is necessary to include in the dynamical equations a representation of wave dissipation from wave breaking and related processes, in order that a forced-damped equilibrium balance can be established. For simplicity, this dissipation is represented as linear damping of the vector momentum with a constant, isotropic damping coefficient. The main motivation for this simple representation is that it allows the derivation of analytical results that should provide at least qualitative physical insight into the potential effects of damping on the equilibrium-sea drift. The physical interpretation of this form of damping is discussed in Section 5. The inclusion of this damping distinguishes the dynamical setting from, for example, the inviscid rotating waves considered by Hasselmann (1970) and Xu and Bowen (1994).

If the motion field is assumed to be two-dimensional, with all wave crests and troughs perpendicular to the x-axis, the linear wave equations with rotation and linear drag are:

$$\frac{\partial u}{\partial t} - fv = -\frac{1}{\rho_0}\frac{\partial p}{\partial x} - \Gamma_S u, \tag{1}$$

$$\frac{\partial v}{\partial t} + fu = -\Gamma_S v, \tag{2}$$

$$\frac{\partial w}{\partial t} = -\frac{1}{\rho_0}\frac{\partial p}{\partial z} - g - \Gamma_S w, \tag{3}$$

$$\frac{\partial u}{\partial x} + \frac{\partial w}{\partial z} = 0, \tag{4}$$

with surface boundary conditions

$$w = \frac{\partial \zeta}{\partial t} \quad \text{and} \quad p = p_a(x,t) \quad \text{at} \quad z = \zeta(x,t). \tag{5}$$

All variables in (1)-(4) are required also to vanish as $z \longrightarrow -\infty$. In (1)-(5), (u,v,w) are the velocities in the (x,y,z) directions, respectively, p is the pressure, f is the constant Coriolis parameter, ρ_0 is a constant reference density, g is the constant acceleration of gravity, Γ_S is a constant damping coefficient, ζ is the free-surface displacement, and p_a is the atmospheric pressure at the free surface. In Section 4, Γ_S will be related to the inverse of a wind-sea equilibration timescale T_S, which in general will be much longer than the timescale $T_\sigma \approx 2\pi/\sigma$ for surface gravity wave oscillations with frequency σ, so that $\Gamma_S/\sigma \ll 1$.

The damped rotating wave solutions of (1)-(5) with $\Gamma_S \neq 0$ retain the two-dimensional structure of the inviscid wave described by Hasselmann (1970) and Xu and Bowen (1994). The velocity variables may be eliminated from (1)-(4) to obtain the pressure evolution equation,

$$\left(\frac{\partial}{\partial t} + \Gamma_S\right)^2 \left(\frac{\partial^2 p}{\partial x^2} + \frac{\partial^2 p}{\partial z^2}\right) + f^2 \frac{\partial^2 p}{\partial z^2} = 0. \tag{6}$$

Following Hasselmann (1970) or Komen et al. (1994), let

$$(u, v, w, \zeta, p + g\rho_0 z) = [\hat{U}(z,t), \hat{V}(z,t), \hat{W}(z,t), Z(t), \hat{P}(z,t)]\, e^{ikx} \tag{7}$$

in (1)-(6). It follows from the surface boundary condition (5) that

$$\hat{P}(z=\zeta,t) = P_a(t) + \rho_0 g Z(t) \quad \text{where} \quad P_a(t)e^{ikx} = p_a(x,t), \tag{8}$$

with the usual interpretation of the complex notation for the wave phase structure. With rotation, it is necessary to allow an independent vertical decay scale m, so that

$$[\hat{U}(z,t), \hat{V}(z,t), \hat{W}(z,t), \hat{P}(z,t)] = [U(t), V(t), W(t), P(t)]\, e^{mz}, \tag{9}$$

where from (5) now also

$$W = \frac{dZ}{dt} \tag{10}$$

$$P = P_a + \rho_0 g Z, \tag{11}$$

and the surface boundary conditions on $\hat{W}$ and $\hat{P}$ have been applied at $z = 0$, consistent with the linear approximation to the dynamics. The vertical momentum balance (3) can be evaluated at the surface, using the boundary conditions (10)-(11) and with (7)-(9), to obtain a single evolution equation for $Z(t)$,

$$\left(\frac{d}{dt} + \Gamma_S\right)\frac{dZ}{dt} = -gm(Z + Z_a), \tag{12}$$

where

$$Z_a = \frac{1}{\rho_0 g} P_a. \tag{13}$$

The rotating linear wave solutions with complex frequency $\tilde{\sigma}$,

$$Z(t) = Z_0 e^{-i\tilde{\sigma}t+mz}, \quad \hat{P}(z,t) = P(t)\,e^{mz} = P_0 e^{-i\tilde{\sigma}t+mz}, \tag{14}$$

then must have, from (6),

$$(\Gamma_S - i\tilde{\sigma})^2(m^2 - k^2) + f^2 m^2 = 0 \tag{15}$$

and, from the surface boundary conditions (10)-(11),

$$-i\tilde{\sigma}(\Gamma_S - i\tilde{\sigma})Z = -gm(Z + Z_a). \tag{16}$$

The vertical decay scale m may be eliminated between (15) and (16), and setting $Z_a = 0$ then gives the dispersion relation $\tilde{\sigma} = \Sigma(k)$ for the damped, rotating free waves, which are the homogeneous solutions of (1)-(5). To first order in Γ_S/σ and f^2/σ^2, the resulting vertical decay scale m and complex frequency $\tilde{\sigma}$,

$$m = \left(1 + \frac{f^2}{2\sigma^2}\right) k \approx k, \quad \tilde{\sigma} = \left(1 + \frac{f^2}{4\sigma^2}\right) (gm)^{1/2} - \frac{1}{2} i \Gamma_S \approx \sigma - i r_S, \tag{17}$$

have rotational corrections of order f^2/σ^2, where

$$\sigma = (gk)^{1/2} \tag{18}$$

is the usual, inviscid, deep-water gravity wave frequency and

$$r_S = \frac{1}{2} \Gamma_S \tag{19}$$

is the decay rate for the damped free waves. The f^2/σ^2 terms in (17) are negligible for wind-sea waves, which generally have periods $T_\sigma = 2\pi/\sigma \leq 10$ s, and are much smaller than the neglected corrections of order Γ_S^2/σ^2. Thus, the vertical decay scale and free-wave frequency may be considered unchanged from the non-rotating case: $m = k$ and $\sigma = (gm)^{1/2} = (gk)^{1/2}$.

The corresponding solutions for (U, V, W) with time dependence as in (14) can be computed from the solutions (14)-(18) for (Z, P) using (10), (11) and (13) with $Z_a = 0$, and the cross-wind momentum and mass conservation equations,

$$\left(\frac{d}{dt} + \Gamma_S\right) V = -fU, \quad W = -iU. \tag{20}$$

The inviscid ($\Gamma_S = 0$) versions of these linear, rotating, wave solutions and the corresponding exact, inviscid expressions for m and $\tilde{\sigma}$ were obtained by Xu and Bowen (1994).

b. Inviscid mean wave drift and Coriolis force balance

An Eulerian momentum balance for the mean wave drift can be derived in two ways: for a fixed-depth (relative to the mean sea surface) Eulerian mean, in which the wave drift is confined between the trough and crest of the wave (Hasselmann 1970; Phillips 1977), and for a mass-weighted, surface-conforming, lateral spatial mean, in which the wave drift has the same vertical profile as the classical Stokes-drift Lagrangian mean (Samelson 2022). The derivation of these inviscid wave-drift balances, equivalent to those derived by Hasselmann (1970), is summarized here, preliminary to consideration of the forced-damped balances in Section 4. The traditional, fixed-depth Eulerian mean taken below the wave troughs does not capture this wave drift or the associated momentum balance.

Consider the inviscid ($r_S = 0$) free-wave solution with free surface displacement

$$\zeta(x,t) = \mathrm{Re}\{Z(t)e^{ikx}\} = a\cos(kx - \sigma t), \tag{21}$$

where $\mathrm{Re}\{\cdot\}$ denotes the real part and $a \ll k^{-1}$. The corresponding downwind wave velocity $u(x,z,t)$ is

$$u(x,z,t) = \mathrm{Re}\{U(t)\,e^{kz}\} = \mathrm{Re}\{iW(t)\,e^{kz}\} = \mathrm{Re}\{i\frac{dZ}{dt}\,e^{kz}\} = \sigma a e^{kz}\,\cos(kx - \sigma t). \tag{22}$$

In the translating reference frame $(\tilde{x},\tilde{z},\tilde{t})$, where

$$\tilde{x}(x,t) = x - ct, \quad \tilde{z} = z, \quad \tilde{t} = t, \tag{23}$$

and $c = \sigma/k$, the downwind velocity $\tilde{u}(\tilde{x},\tilde{z})$ is steady,

$$\tilde{u}(\tilde{x},\tilde{z}) = \sigma a e^{k\tilde{z}}\cos k\tilde{x}. \tag{24}$$

Below the wave troughs, the fixed-depth Eulerian mean U_E of $\tilde{u}$ is zero, because $\tilde{u}$ is periodic in $\tilde{x}$. Between the troughs and crests, however, the fixed-depth Eulerian mean U_E does not vanish:

$$U_E(|\tilde{z}| \le a) = \frac{1}{2\pi}\int_{-\theta_\zeta(\tilde{z})}^{\theta_\zeta(\tilde{z})} \sigma a\cos\theta\,d\theta = \frac{\sigma a}{\pi}\left(1 - \frac{\tilde{z}^2}{a^2}\right)^{1/2}, \tag{25}$$

where $\theta = k\tilde{x}$ and $\theta_\zeta(\tilde{z}) = \arccos(|\tilde{z}|/a)$. In (25), the approximation

$$\tilde{u}(\tilde{x},|\tilde{z}| \le a) \approx \sigma a\,(1 + k\tilde{z})\cos k\tilde{x} \approx \sigma a\cos k\tilde{x} \tag{26}$$

has been made, consistent with the small-slope condition $ka \ll 1$. From (20) with $\Gamma_S = 0$, the cross-wind velocity $v(x,z,t)$ is out of phase with $u(x,z,t)$ and has zero mean between the troughs and crests:

$$v(x,z,t) = fae^{kz}\ \sin(kx - \sigma t), \tag{27}$$

so that

$$\tilde{v}(\tilde{x},\tilde{z}) = fae^{k\tilde{z}} \sin k\tilde{x}, \tag{28}$$

and

$$V_E(|\tilde{z}| \le a) = \frac{1}{2\pi}\int_{-\theta_\zeta(\tilde{z})}^{\theta_\zeta(\tilde{z})} fa \sin\theta\, d\theta = \frac{fa}{2\pi}(\cos\theta)\Big|_{-\theta_\zeta(\tilde{z})}^{\theta_\zeta(\tilde{z})} = 0. \tag{29}$$

The along-crest acceleration, however, is in phase with the free-surface displacement and down-wind velocity,

$$\frac{\partial v}{\partial t} = \frac{\partial}{\partial t}\tilde{v}[\tilde{x}(x,t),\tilde{z}] = -c\frac{\partial \tilde{v}}{\partial \tilde{x}} = -ckfa\cos k\tilde{x}. \tag{30}$$

Consequently, and consistent with the momentum balance (20) from which $v(x,z,t)$ was obtained, the mean along-crest acceleration is not zero between the troughs and crests, but instead precisely balances the mean Coriolis force associated with the mean wave drift U_E:

$$\frac{\partial V_E}{\partial t}(|\tilde{z}| \le a) = \frac{1}{2\pi}\int_{-\theta_\zeta(\tilde{z})}^{\theta_\zeta(\tilde{z})}\left(-c\frac{\partial \tilde{v}}{\partial \tilde{x}}\right) d\theta = -f\frac{\sigma a}{\pi}\left(1 - \frac{\tilde{z}^2}{a^2}\right)^{1/2} = -fU_E(|\tilde{z}| \le a). \tag{31}$$

A physical interpretation of this balance is that the Coriolis force from the fixed-depth mean downwind wave velocity U_E drives and is absorbed by the change in v from the leading to the trailing edge of the wave at each fixed depth between trough and crest. This change in v appears directly through the integral in (31),

$$\int_{-\theta_\zeta(\tilde{z})}^{\theta_\zeta(\tilde{z})}\left(-c\frac{\partial \tilde{v}}{\partial \tilde{x}}\right) d\theta = -ck\int_{-k^{-1}\theta_\zeta(\tilde{z})}^{k^{-1}\theta_\zeta(\tilde{z})}\frac{\partial \tilde{v}}{\partial \tilde{x}}\, d\tilde{x} = -\sigma\int_{v_-}^{v_+} d\tilde{v} = -\sigma(v_+ - v_-), \tag{32}$$

where

$$v_\pm = \tilde{v}[\pm k^{-1}\theta_\zeta(\tilde{z}),\tilde{z}] = \pm fa\sin\left[k^{-1}\theta_\zeta(\tilde{z})\right] = \pm fa\left(1 - \frac{\tilde{z}^2}{a^2}\right)^{1/2} \tag{33}$$

are the leading-edge and trailing-edge values of v, respectively, at the fixed depth $\tilde{z} = z$ between the trough and crest.

An alternative Eulerian mean that is more amenable to physical interpretation may be computed in surface-conforming, orthogonal curvilinear coordinates, provided that care is taken to weight the transformed variables properly by mass (Samelson 2022). In the translating frame, the orthogonal curvilinear coordinates for the linear wave motion (21) are (Phillips 1977)

$$\xi(\tilde{x},\tilde{z}) = \tilde{x} - ae^{k\tilde{z}}\sin k\tilde{x}, \tag{34}$$

$$\eta(\tilde{x},\tilde{z}) = \tilde{z} - ae^{k\tilde{z}}\cos k\tilde{x}. \tag{35}$$

The transformation (34)-(35) may be inverted to the same accuracy, giving

$$\tilde{X}(\xi,\eta) = \xi + ae^{k\eta}\sin k\xi, \tag{36}$$

$$\tilde{Z}(\xi,\eta) = \eta + ae^{k\eta}\cos k\xi. \tag{37}$$

Again to the same accuracy, the Jacobian determinant $J(\tilde{X},\tilde{Z})$ of the transformation $(\tilde{x},\tilde{z}) = [\tilde{X}(\xi,\eta),\tilde{Z}(\xi,\eta)]$ is

$$J(\tilde{X},\tilde{Z}) = 1 + 2kae^{k\eta}\cos k\xi. \tag{38}$$

To second order in wave slope, the mass-weighted, surface-conforming mean (Samelson 2022) of a function $\psi(\xi,\eta) = \psi_0 e^{k\eta}\cos k\xi$ on an arbitrary η surface is then

$$\Psi(\eta) = -\frac{k}{2\pi}\int_0^{2\pi/k} \psi(\xi,\eta)\,J(\tilde{X},\tilde{Z})\,d\xi = ka\psi_0 e^{2k\eta}, \tag{39}$$

The mean depth $\bar{Z}(\eta)$ of a given η surface is, similarly,

$$\bar{Z}(\eta) = \frac{k}{2\pi}\int_0^{2\pi/k} \tilde{Z}(\xi;\eta)\,J(\tilde{X},\tilde{Z})\,d\xi = \eta + ka^2\left(e^{2k\eta} - 1\right), \tag{40}$$

and the surface-conforming mean wave drift $U_S(\bar{Z})$ derived by Samelson (2022) for the velocity $u(\tilde{X},\tilde{Z}) = \sigma ae^{k\tilde{Z}}\cos k\tilde{X} = u(\xi,\eta) = \sigma ae^{k\eta}\cos k\xi$ is, to second order in ka,

$$U_S(\bar{Z}) = \sigma ka^2 e^{2k\bar{Z}}, \tag{41}$$

which in turn is equal to the classical Lagrangian mean Stokes drift (e.g., Phillips 1977; van den Bremer and Breivik 2018).

Following the same approach as for (36)-(41), and using (39), shows that the mass-weighted, surface-conforming mean of the inviscid cross-wind velocity $\tilde{v}$ in (28) vanishes identically, while that of the inviscid acceleration $\partial v/\partial t$ in (30) does not vanish and instead exactly balances the Coriolis force from the mean downwind drift at each depth,

$$\overline{\frac{\partial v}{\partial t}} = \left(kae^{2k\tilde{Z}}\right) \times (-ckfa) = -f\sigma ka^2 e^{2k\tilde{Z}} = -fU_S. \tag{42}$$

A physical interpretation of the cross-wind momentum balance in the surface-conforming mean is that the greater Coriolis force in the crest, where the coordinate is stretched vertically and the mass is concentrated, causes a velocity acceleration equal and opposite to that caused by the weaker Coriolis force below the trough, where the coordinate is compressed vertically and there is less mass per vertical coordinate unit.

Thus, in both Eulerian means, the mean Coriolis force associated with the wave momentum (i.e., the wave drift or, from the Lagrangian perspective, the Stokes drift) as computed from inviscid linear theory is from this perspective balanced within the fast timescale linear wave dynamics. Consequently, if the analysis were complete at this point, there would be no effect of this Coriolis force from the mean drift on the mean flow, i.e., no "Stokes-Coriolis" term should appear in the wave-averaged equations. However, both the Coriolis force and the acceleration terms are of second order in the small parameter ka. Therefore, it is necessary to compute the nonlinear acceleration terms, which are nominally of this same order. This calculation was done by Hasselmann (1970) and Xu and Bowen (1994), who found that the mean nonlinear acceleration term in the cross-wind momentum equation is, at the same second order in ka, equal to the Coriolis force from the mean wave drift. This mean nonlinear acceleration does not balance the mean wave-drift Coriolis force but instead adds to it. In effect, this restores the mean wave-drift Coriolis force in the mean cross-wind momentum balance.

Because the nonlinear acceleration terms are nominally of second order in ka, the associated Eulerian means can be computed directly at fixed depth throughout the mean water column, and the third-order terms deriving from correlations with the fluctuating sea surface can be neglected.

In the cross-wind momentum equation, the nonlinear acceleration terms are

$$u\frac{\partial v}{\partial x}+w\frac{\partial v}{\partial z}=\frac{\partial}{\partial x}(uv)+\frac{\partial}{\partial z}(vw). \tag{43}$$

Since the product uv is periodic in x at fixed depth, the fixed-depth mean of the first term vanishes, and the total mean cross-wind nonlinear acceleration is

$$\overline{\frac{\partial}{\partial z}(vw)}=\frac{k}{2\pi}\int_0^{2\pi/k}\frac{\partial}{\partial z}\left(fae^{kz}\sin k\tilde{x}\times\sigma ae^{kz}\sin k\tilde{x}\right)d\tilde{x}=f\sigma k^2ae^{2kz}=fU_S, \tag{44}$$

as shown by Hasselmann (1970) and Xu and Bowen (1994). The mean local time derivative of the wave motion $v(x,z,t)$ balances the Coriolis force from the mean wave-drift according to (42), so the inclusion of the nonlinear acceleration (44) in the full second-order mean cross-wind momentum equation leaves an imbalance. This imbalance must be taken up by an additional local acceleration $\partial(V_2e^{2kz})/\partial t$ of a mean second-order drift $V_2(t)e^{2kz}$, so that the full mean second-order horizontal momentum balance is

$$\overline{\frac{\partial v}{\partial t}}+\frac{\partial V_2}{\partial t}e^{2kz}+\overline{\frac{\partial}{\partial z}(vw)}+fU_S=0, \tag{45}$$

which, on using $\overline{\partial v/\partial t}=-fU_S=-\overline{\partial/\partial z(vw)}$ from (42) and (44), simplifies to

$$\frac{\partial V_2}{\partial t}e^{2kz}+fU_S=0. \tag{46}$$

In the downwind momentum equation, the nonlinear acceleration terms are

$$u\frac{\partial u}{\partial x}+w\frac{\partial u}{\partial z}=\frac{\partial}{\partial x}(u^2)+\frac{\partial}{\partial z}(uw), \tag{47}$$

both of which vanish in the fixed-depth Eulerian mean, because $uw\propto\cos k\tilde{x}\times\sin k\tilde{x}\propto\sin 2\tilde{x}$, so there is no nonlinear correction to the mean downwind momentum balance. The non-rotating terms in the inviscid downwind momentum equation balance exactly,

$$\frac{\partial u}{\partial t}=-\frac{1}{\rho_0}\frac{\partial p}{\partial x}=\sigma^2a\sin(kx-\sigma t), \tag{48}$$

so an additional local acceleration $\partial(U_2 e^{2kz})/\partial t$ of a mean second-order downwind drift $U_2(t)e^{2kz}$ must likewise be allowed to balance the Coriolis force from the induced second-order drift $V_2 e^{2kz}$ in the full mean second-order downwind momentum balance. With the Coriolis force from this additional downwind drift included in the cross-wind momentum equation, the full mean second-order horizontal momentum balance is,

$$\frac{\partial U_2}{\partial t} e^{2kz} - f V_2 e^{2kz} = 0, \quad \frac{\partial V_2}{\partial t} e^{2kz} + f(U_S + U_2 e^{2kz}) = 0. \tag{49}$$

For steady mean wave drift U_S, this recovers the classical result of Hasselmann (1970) that there must be a steady mean upwind drift $(U_{20}e^{2kz}, V_{20}) = (-U_S, 0)$ that compensates the wave drift, plus homogeneous solutions in the form of inertial oscillations with $U_2 + iV_2 \propto e^{-ift}$. Nonlinear corrections to the linear kinematic surface boundary condition (5) must also be considered but both vanish in the mean, because the variable pairs in each of the two quadratic correction products, $u(\partial\zeta/\partial x)$ and $\zeta(\partial w/\partial z)$, are out of phase with one another.

3. Forced-damped mean wave drift and Coriolis force balance

With forcing and damping, i.e., with $\Gamma_S > 0$ in (1)-(3) and $p_a \neq 0$ in (5), the balances and phase relations change such that monochromatic equilibrium-sea solutions of (1)-(5) exist in which inertial oscillations are absent and the Coriolis forces from the mean wave drift are balanced by drag on the mean drift. The forced-damped equations can be solved by separation into homogeneous and particular solutions, where the homogeneous solutions are now the damped free waves described in Sec. 2.a, for which rotation can be ignored to first order in the downwind momentum balance.

To develop a forced-damped solution, it is necessary to specify the pressure forcing, which implicitly assumes a pre-existing wave disturbance relative to which the pressure phase can be defined. Consider a surface pressure disturbance $p_a(x,y,t)$ that is correlated with the wave slope for the inviscid free-wave solution $\zeta(x,t) = a\cos(kx - \sigma t)$ given in (21),

$$p_a(x,y,t) = -P_{a0}\sin\theta(x,t), \quad \theta(x,t) = kx - \sigma t, \tag{50}$$

where P_{a0} is a suitable positive constant. This gives a mean force F_P on the propagating wave that may be taken to be a fraction b_0 of the wind stress τ_0:

$$F_P = \frac{1}{2\pi}\int_0^{2\pi} p_a(x,t)\,\frac{\partial \zeta}{\partial x}\,d\theta = \frac{1}{2\pi}\int_0^{2\pi} kaP_{a0}\sin^2\theta\,d\theta = \frac{1}{2}kaP_{a0} = b_0\tau_0. \tag{51}$$

The correlation of the pressure disturbance with the vertical wave motion $w(x, z = 0, t) = \sigma a \sin\theta(x,t)$ at the surface will also provide an energy flux F_K that drives the wave field:

$$\begin{aligned} F_K &= -\frac{1}{2\pi}\int_0^{2\pi} p_a(x,t)\,w(x,z=0,t)\,dx = \frac{1}{2\pi}\int_0^{2\pi} \sigma a P_{a0}\sin^2\theta\,d\theta \\ &= \frac{1}{2}\sigma a P_{a0} = cF_P = b_0\,c\,\tau_0, \end{aligned} \tag{52}$$

in agreement with standard wave energy growth scaling. If the wind-stress fraction $b_0\tau_0$ is taken to depend linearly on the wave slope, so that

$$b_0 = b_2\,ka, \tag{53}$$

as suggested by, for example, the measurements by Buckley et al. (2020), then the pressure forcing amplitude

$$P_{a0} = \frac{2b_0\tau_0}{ka} = 2b_2\tau_0 \tag{54}$$

is independent of the wave slope.

Solutions of (12) with $m = k$ are again sought but now, for the forced-damped case, with $Z_a = P_a/(\rho_0 g) \neq 0$ for $P_a = -iP_{a0}e^{-i\sigma t}$ from (50) in the equivalent complex notation and with $\Gamma_S \neq 0$. The forcing at the real frequency $\sigma = (gk)^{1/2}$ is not resonant in the damped case, and a particular solution Z_p of (12) can be directly obtained, for which

$$\zeta_p(x,t) = \mathrm{Re}\{Z_p(t)\,e^{ikx}\} = a_p\cos\theta, \tag{55}$$

where

$$a_p = \frac{\sigma P_{a0}}{\rho_0 g\Gamma_S} = \frac{\sigma}{\Gamma_S}\,\frac{2b_2\tau_0}{\rho_0 g} \tag{56}$$

is the amplitude of the forced free-surface displacement response for the wave-slope dependent b_0 (53). If b_0 is taken to be constant, independent of ka, then (12) becomes nonlinear in the wave amplitude but a particular solution with constant a_p can still be sought, for which (56) will be replaced by

$$a_p = \frac{\sigma}{\Gamma_S}\frac{2b_0\tau_0}{\rho_0 g k a_p}, \tag{57}$$

which implies

$$a_p = \left(\frac{2b_0\tau_0}{\rho_0\sigma\Gamma_S}\right)^{1/2} \tag{58}$$

The two expressions for a_p are equivalent if the constant value b_0 in (58) is equal to $b_2\, ka_p$ for b_2 in (53) and (56).

From (7)-(11), the corresponding solution for the forced pressure disturbance is

$$p'_p(x,z,t) = \mathrm{Re}\{\hat{P}_p(z,t)\, e^{ikx}\} = \rho_0 g a_p e^{kz}\left(\cos\theta - \frac{\Gamma_S}{\sigma}\sin\theta\right). \tag{59}$$

With $U = iW = i\,(dZ/dt) = \sigma Z$, the downwind and vertical velocities can be written as,

$$u_p(x,z,t) = \sigma a_p\, e^{kz}\cos\theta, \quad w_p(x,z,t) = \sigma a_p\, e^{kz}\sin\theta. \tag{60}$$

From the cross-wind momentum balance $(d/dt + \Gamma_S)V = (-i\sigma + \Gamma_S)V = -fU$, it follows that

$$v_p(x,z,t) = -f\sigma a_p(\sigma^2 + \Gamma_S^2)^{-1}\, e^{kz}(\Gamma_S\cos\theta - \sigma\sin\theta). \tag{61}$$

The surface-conforming mean wave-correlated drift and pressure forcing are then

$$\overline{u_p} = \sigma a_p \times k a_p e^{2kz} = \sigma k a_p^2\, e^{2kz}, \tag{62}$$

$$\overline{v_p} = -f\sigma a_p(\sigma^2+\Gamma_S^2)^{-1}\Gamma_S \times k a_p e^{2kz} = -\left(\frac{f\Gamma_S}{\sigma^2+\Gamma_S^2}\right)\overline{u}_p, \tag{63}$$

$$\overline{-\frac{1}{\rho_0}\frac{\partial p'_p}{\partial x}} = g a_p \frac{\Gamma_S}{\sigma} k \times k a_p e^{2kz} = \Gamma_S\,\overline{u}_p. \tag{64}$$

The mean downwind drift depends on the forced free-surface displacement parameters in the same way as in the inviscid free-wave case and so is again equivalent to the Lagrangian-mean Stokes drift. The mean cross-wind drift is not zero in the damped case but is of order $f\Gamma_S/\sigma^2 \ll 1$ relative to the mean downwind drift. The implicit neglect of the Coriolis force from the mean cross-wind drift in the downwind momentum equation is consistent, as it would be of order $f^2/\sigma^2 \ll 1$ relative to the mean drag and pressure forcing terms.

As in the inviscid case, it is necessary to consider the second-order nonlinear acceleration terms, where the small wave-slope parameter is now ka_p. The spatial-mean nonlinear terms again vanish for the downwind momentum balance but not for the cross-wind momentum balance, where now

$$\overline{\frac{\partial}{\partial z}(v_p w_p)} = \frac{k}{2\pi}\int_0^{2\pi/k} \frac{\partial}{\partial z}\left[f a_p \left(1+\frac{\Gamma_S^2}{\sigma^2}\right)^{-1} e^{kz}\sin k\tilde{x} \times \sigma a_p e^{kz}\sin k\tilde{x}\right] d\tilde{x}, \tag{65}$$

so that

$$\overline{\frac{\partial}{\partial z}(v_p w_p)} = \left(1+\frac{\Gamma_S^2}{\sigma^2}\right)^{-1} f\sigma k^2 a_p e^{2kz} = \left(1+\frac{\Gamma_S^2}{\sigma^2}\right)^{-1} f\overline{u}_p \approx f\overline{u}_p, \tag{66}$$

essentially as in the free-wave case. Thus, an additional mean cross-wind drift V_2 again must be allowed in the cross-wind momentum equation, which again will induce a Coriolis force and downwind drift U_2 in the downwind momentum equation. In this case, however, the additional mean drift (U_2, V_2) will appear in the drag terms, so that the full forced-damped mean drift equations are

$$-fV_2e^{2kz} = -\overline{\frac{1}{\rho_0}\frac{\partial p_p'}{\partial x}} - \Gamma_S(\overline{u}_p + U_2e^{2kz}), \quad f(\overline{u}_p + U_2e^{2kz}) = -\Gamma_S V_2 e^{2kz}. \tag{67}$$

Defining the mean wave-drift velocity vector as

$$\mathbf{U}_S = (U_S, V_S) = (\overline{u}_p + U_2e^{2kz}, V_2e^{2kz}), \tag{68}$$

gives the mean forced-damped drift momentum equations as

$$-fV_S = -\overline{\frac{1}{\rho_0}\frac{\partial p_p'}{\partial x}} - \Gamma_S U_S, \quad fU_S = -\Gamma_S V_S. \tag{69}$$

These equations may be solved for $\mathbf{U}_S$, which gives

$$\mathbf{U}_S = \overline{u}_p \cos\gamma_S\,(\cos\gamma_S, -\sin\gamma_S), \tag{70}$$

where the rotation angle from downwind is

$$\gamma_S = \arctan\left(\frac{f}{\Gamma_S}\right). \tag{71}$$

If the equilibrium-sea timescale $T_S \approx 1/\Gamma_S$ is a substantial fraction of the inertial timescale $1/f$, then the resulting rotation of the mean wave-drift from downwind, $\gamma_S \approx \arctan(fT_S)$, will likewise be substantial. The magnitude of the vector drift will then also be reduced by the factor $|\cos\gamma_S| < 1$.

4. Equilibrium-sea timescales and Stokes drift angle

a. Monochromatic forced-damped estimate

An estimated equilibrium-sea equilibration timescale T_S can be obtained from the monochromatic forced-damped solution (55)-(60) by setting $T_S = 1/\Gamma_S$ and equating the mean squared amplitude $\frac{1}{2}a_p^2$ to observed estimates $\overline{\zeta^2}$ of mean squared displacements for equilibrium-sea conditions. From (56) with $b_0 = b_2 k a_p$, or from (58), and with $\sigma = g/c$, the resulting equilibration timescale is,

$$T_S = \frac{1}{\Gamma_S} = \frac{\rho_0 g \overline{\zeta^2}}{b_0 c \tau_0}. \tag{72}$$

The resulting inferred damping rate $\Gamma_S = 1/T_S$ is equivalent to the standard expression for wave growth rate obtained as the ratio of the rate of wave energy growth with time, $dE/dt = b_0 c \tau_0$, to the wave energy, $E = \frac{1}{2}\rho_0 g a_p^2 = \rho_0 g \overline{\zeta^2}$.

To obtain numerical estimates of Γ_S and T_S, representative values of the stress fraction b_0 and phase speed c (or, equivalently, the transfer velocity $b_0 c$) and $\overline{\zeta^2}$ must be specified as a function of the 10-m wind speed U_{10N}. A simple approach is to let $a_p = (2\overline{\zeta^2})^{1/2} = H_s/2$ and $c = c_p$, where the equilibrium-sea significant wave-height $H_s(U_{10N})$ and peak-wavelength phase speed $c_p(U_{10N})$ are taken from the Samelson (2022) fully-developed sea and bulk-flux wave state relations (Fig. 1a-g). For b_0 as in (53) with $b_2 = 5$ as suggested by the measurements of Buckley et al. (2020), the resulting equilibrium-sea timescale,

$$T_S(U_{10N}) = \frac{\frac{1}{8}\rho_0 g H_s^2}{b_0 c_p \tau_0} \tag{73}$$

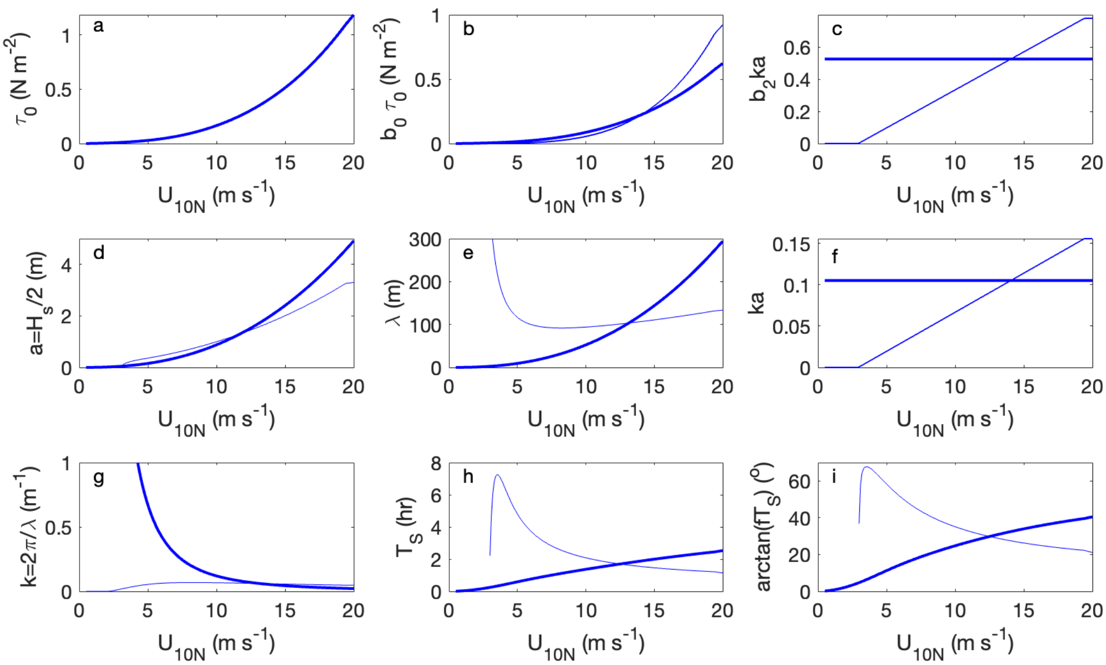

Fig. 1. Parameters vs. 10-m neutral wind speed (m s^{-1}) for T_S values from (73) computed for fully-developed sea (thick line) and bulk-flux (thin) wave states from Samelson (2022): (a) total wind stress τ_0, (b) wave-forcing wind-stress fraction $b_0\tau_0$, (c) wind stress fraction $b_0 = b_2 ka$ from (53) with $b_2 = 5$, (d) wave amplitude $a_p = H_s/2$, (e) spectral-peak wavelength λ_p, (f) wave slope ka, (g) spectral-peak wavenumber k_p, (h) equilibration timescale T_S, (i) mean wave-drift rotation angle $\gamma_S = \arctan(fT_S)$.

is a substantial fraction of the mid-latitude inertial timescale $1/f$ for $U_{10N} > 3$ m s^{-1} (Fig. 1h), and the implied rotation of the mean wave-drift from downwind, $\gamma_S = \arctan(fT_S)$, can be several tens of degrees or more at mid-latitudes (Fig. 1i).

A Lagrangian wave-drift momentum timescale estimate, consistent with (72), can be obtained from time-dependent Lagrangian-mean expressions derived by Pizzo and Wagner (2025) in their asymptotic analysis of wave growth from pressure forcing for the non-rotating case. Equating their second-order drift (Pizzo and Wagner 2025, their eq. 52), which grows quadratically in time, to the standard Stokes drift $\epsilon^2\omega ka^2 e^{2kz}$ for their wave amplitude ϵa, with $P_{a0} = 2b_0\tau_0/(k\epsilon a)$ from (51), gives a timescale

$$T_L = \frac{\epsilon a}{\epsilon \mathcal{A}\omega} = \frac{\epsilon a}{(2g\rho_0)^{-1}P_{a0}(gk)^{1/2}} = \frac{2\rho_0 g^{1/2}\epsilon a}{k^{1/2}P_{a0}} = 2T_S, \qquad (74)$$

where, as in Pizzo and Wagner (2025), $\epsilon\mathcal{A} = P_{a0}/(2g\rho_0)$ is an equivalent vertical free-surface displacement for the pressure forcing and the dimensionless small parameter ϵ has been introduced to scale the wave amplitude and the pressure forcing. The factor of 2 difference between (74) and (72) evidently arises because the Pizzo and Wagner (2025) pressure forcing incorporates the growth of the wave amplitude from a small value, whereas (72) uses an equilibrated wave amplitude.

b. Empirical wave-growth estimate

Observations of growing wind-driven waves with wavenumber k are generally consistent with the growth rate suggested by Plant (1982), denoted here by β_k:

$$\beta_k \approx 0.04 \frac{v_*^2}{c^2} \sigma. \tag{75}$$

In (75), c/v_* is the wave-age parameter and $v_* = (\tau_0/\rho_a)^{1/2}$ is the air friction velocity for air density ρ_a. In an equilibrium sea, the mean rates of energy input and loss for waves in the equilibrium range must be approximately equal, differing only by the spectral flux of energy between wavenumbers within the range (Phillips 1985). Thus, the wave growth rate β_k can be taken as an empirical estimate of the damping rate Γ_S, giving a spectral equilibrium-sea timescale T_k as

$$T_k = \frac{1}{\beta_k} = 25 \frac{c^2}{v_*^2} \frac{1}{\sigma} = 25\, v_*^{-2} g^{1/2} k^{-3/2}. \tag{76}$$

The spectral flux may have magnitude as large as one-third of the wind input in the equilibrium range (Ardhuin et al. 2010) but the growth and dissipation rates will still be similar enough that T_k may be taken here as an estimate of both timescales.

The spectral timescale T_k is generally smaller than T_S computed for the monochromatic model, but can still be a substantial fraction of the mid-latitude inertial timescale $1/f$. Thus, for $\Gamma_S = 1/T_k$, the resulting clockwise rotation angle γ_k, where

$$\gamma_k = \arctan(f T_k), \tag{77}$$

of the mean wave-drift from downwind can be up to several tens of degrees at mid-latitudes (Fig. 2).

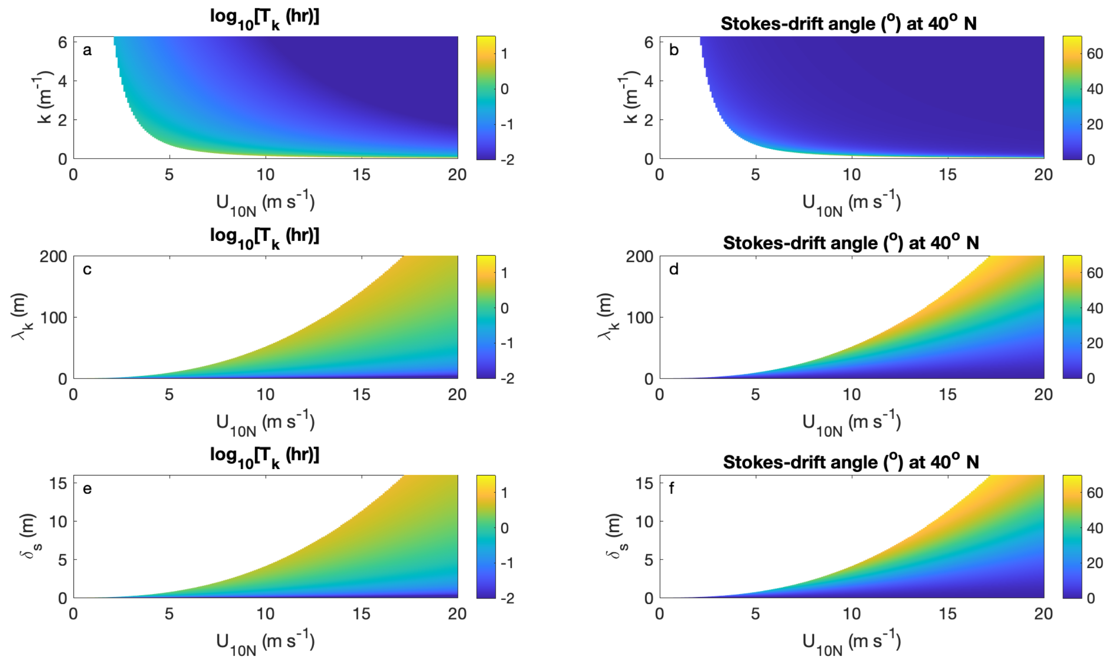

Fig. 2. (a,c,e) Base-10 logarithm of spectral timescale T_k in units of hours and (b,d,f) clockwise wind-relative Stokes drift angle $\gamma_k = \arctan(fT_k)$ for Coriolis parameter f at 40°N for damping on spectral timescale T_k vs. 10-m wind speed and (a,b) wavenumber k, (c,d) wavelength $\lambda_k = 2\pi/k$, and (e,f) Stokes-drift depth $\delta_s = 1/(2k) = \lambda_k/(4\pi)$. Values are shown for wavelengths less than the Resio et al. (1999) fully-developed sea spectral-peak wavelength.

c. Mean wave drift angles and profiles

In the monochromatic equilibrium-sea model, the total wind-sea drift is represented by the single drift veloctity profile $\mathbf{U}_S$ (70) at the wavelength k_p, corresponding to the spectral peak at the long-wavelength end of the equilibrium wind-sea spectral range. This drift velocity profile is rotated by the angle γ_k, which is independent of depth and to the right of the wind in the Northern Hemisphere. The peak wavelength λ_p and phase speed c_p used for the monochromatic timescale T_S (73) are, effectively, upper bounds for the corresponding quantities in the spectral estimate T_k (76), because the peak wavelength and phase speed are at the long-wavelength limit of the equilibrium wind-sea spectral range. Thus, the monochromatic rotation angle γ_S is also effectively an upper bound for the rotation angles of the drift in the spectral equilibrium wind-sea range.

In the spectral representation, the timescale T_k and rotation angle γ_k are different for each wavenumber k in the equilibrium range, with longer timescales and larger rotation angles for longer waves. The drift vertical decay scale $\delta_S = 1/(2k) = \lambda/(4\pi)$ increases linearly with wavelength, so the rotation angle increases as the vertical decay scale increases. With the forced-damped drift balance (70) taken to hold at each wavenumber k, the solution may be interpreted as a spectral density by setting the squared amplitude a_p^2 in the scalar drift $\overline{u}_p$ from (62) equal to twice the wavenumber spectrum $\Psi(k)$ of mean-square displacement. With $\Psi(k)$ taken as the two-dimensional equilibrium-range spectrum from Phillips (1985) integrated over direction θ, the equilibrium spectra $\hat{\overline{u}}_p(z;k)$ and $\hat{\mathbf{U}}_S(z;k)$ of the scalar and vector wave drift are

$$\begin{aligned} \hat{\overline{u}}_p(z;k) &= 2\sigma\, k\, \Psi(k) e^{2kz} = 2\beta\, I(p)\, v_*\, k^{-2} e^{2kz} && (78)\\ \hat{\mathbf{U}}_S(z;k) &= = 2\beta\, I(p)\, v_*\, k^{-2} \cos\gamma_k\, e^{2kz}\, (\cos\gamma_k, -\sin\gamma_k), && (79) \end{aligned}$$

where $I(p) = \int_{-\pi/2}^{\pi/2} \cos^p\theta\, d\theta$. The total mean vector drift profile (Fig. 3,4) is then the spectral integral

$$\bar{\mathbf{U}}_S(z) = \int_{k_0}^{k_1} \hat{\mathbf{U}}_S(z;k)\, k\, dk = 2\,\beta\, I(p)\, v_* \int_{k_0}^{k_1} k^{-1} \cos\gamma_k\, e^{2kz}\, (\cos\gamma_k, -\sin\gamma_k)\, dk, \qquad (80)$$

where k_0 and k_1 are the limits of the equilibrium range and

$$\gamma_k = \arctan(f T_k) = \arctan(25 f\, v_*^{-2} g^{1/2} k^{-3/2}). \qquad (81)$$

For wind speeds above 10 m s^{-1}, the magnitude of the total mean vector subsurface drift (80) is attenuated by the rotation, relative to the total scalar drift $\overline{U}_p = \int_{k_0}^{k_1} \hat{\overline{u}}_p\, k\, dk$ obtained from the integral over the equilibrium wavenumber range of $\hat{\overline{u}}_p(z;k)$ from (78). The attenuation is depth-dependent and can be of order 10%-20% in the upper 5 meters (Fig. 3). Note that different representations of the equilibrium range spectrum result in different estimates of the amplitude of the drift; for example, the integrated scalar drift $\overline{U}_p$ is only half as large as the scalar drift estimate from the Breivik et al. (2014) analytical integral of the Phillips (1958) σ^{-5} equilibrium spectrum (Fig. 3a-e).

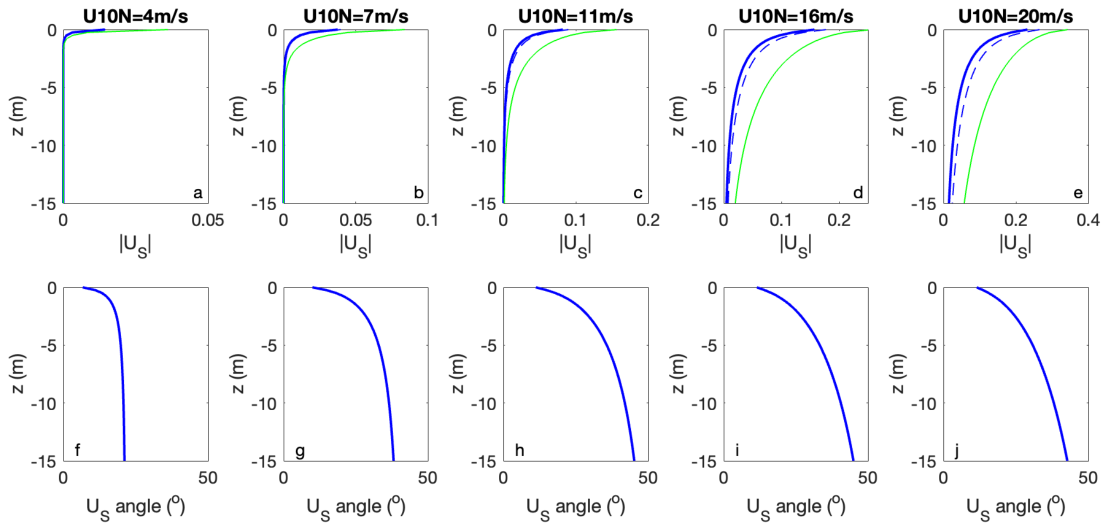

FIG. 3. (a-e) Vector mean Stokes drift magnitude $|\mathbf{U}_S|$ (blue solid lines) from (80), with corresponding integrated scalar drift $\overline{U}_p$ (blue dashed) and (f-j) clockwise wind-relative mean drift angle $\gamma_k = \arctan(fT_k)$ from (81) for Coriolis parameter f at 40°N and damping on spectral timescale T_k vs. depth, for 10-m wind speeds (a,f) 4, (b,g) 7, (c,h) 11, (d,i) 16, (e,j) 20 m s^{-1}. The scalar drift profiles from the Breivik et al. (2014) analytical integral of the Phillips (1958) σ^{-5} equilibrium spectrum are also shown (green lines in a-e).

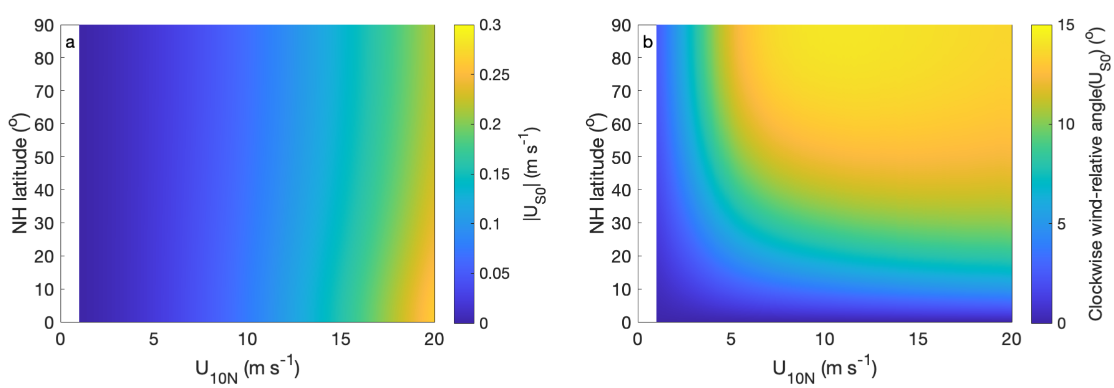

FIG. 4. Clockwise wind-relative angle (°) of vector mean surface Stokes drift $\mathbf{U}_S$ from (80) vs. 10-m wind speed and Northern Hemisphere latitude.

The rotation angle increases with wind speed for wind speeds below approximately 7 m s^{-1} and then is essentially constant for larger wind speeds (Figs. 3,4b). The magnitude of the rotated surface drift is essentially independent of latitude (Fig. 4a) but the rotation angle increases poleward, reaching values of 7° to 12° at subtropical latitudes and up to 15° at high latitudes (Fig. 4b).

5. Equilibrium-sea wind and wave drift

The form of the linear damping terms assumed in (1)-(3) implicitly assumes that surface wave-breaking results in a breakdown of the coherent vertical wave structure, the result of which is to remove the mean drift momentum directly at each depth from the associated wave structure. This flux of momentum out of the wave field at each depth can then consistently be taken to provide a depth-dependent body force that can be inserted as a forcing term into an equilibrium-sea wind-drift model, such as that proposed by Samelson (2022), conserving the total momentum in the combined wave and wind flow. All of the surface stress would then ultimately be deposited as momentum flux into the mean wind drift but the resulting wind-drift and total drift profiles will be different than would be obtained by forcing the wind-drift model alone with the full surface stress. From a physical point of view, the body force from the linear wave-drift damping acts to distribute the surface momentum flux into the near-surface interior through a coherent wave-pressure mechanism rather than turbulence.

An explicit model of the combined equilibrium-sea wind drift and linear-drag wave drift can be constructed by combining the forced-damped wave analysis with the wind-drift model of Samelson (2022), with the latter supplemented by the mean-flow forcing from the linear drag. If the usual wave-averaging assumption is made, according to which the turbulence is effectively frozen on the wave timescale and has no effect on the wave dynamics, then the wave-drift and wind-drift momentum balances can be treated separately. If the fraction b_0 of the total surface wind stress that is deposited into the wave field is given, then the rotating wave-drift balance (70) or (80) can be solved to obtain both the wave drift and the momentum flux from the linear damping of the wave drift. Wind-drift model equations, such as those of Samelson (2022), can then be solved, forced by the remaining fraction $1 - b_0$ of the wind stress at the surface and by the body force that derives from the linear damping of the wave drift. The total drift will consist of the sum of the wave and wind drifts. An outline of an implementation of this approach and two resulting example sets of combined wind-drift and wave-drift profiles are presented here.

The first step is to compute the rotating equilibrium-sea wave-drift profiles as a function of wind speed. The particular implementation chosen for the examples presented here used the spectral form (78)-(81). The lower limit k_0 of the spectral integral (80) was specified as the peak wavenumber $k_p = 2\pi/\lambda_p$ of the fully-developed sea wave-state considered by Samelson (2022), which used the parameterization developed by Resio et al. (1999). The Resio et al. (1999) peak wavelength was used directly, without the adjustment considered by Samelson (2022), so that

$$k_0 = \frac{2\pi}{\lambda_p} = \frac{g}{U_r^2}, \quad \lambda_p = 2\pi\frac{U_r^2}{g}, \quad U_r = 0.516\,(U_{10N})^{1.244}. \tag{82}$$

The upper integration limit k_1 was set in a plausible but ad-hoc manner to satisfy the condition that the total parameterized wave-breaking drag was less than the wind stress, i.e., to guarantee $b_0 < 1$. The profile of pressure forcing on the wave field was computed from (64) and (78) as the spectral integral

$$F_w(z) = \int_{k_0}^{k_1} \overline{\widehat{-\frac{1}{\rho_0}\frac{\partial p_p'}{\partial x}}}(z;k)\,k\,dk = \int_{k_0}^{k_1} \Gamma_k \hat{\bar{u}}_p(z;k)\,k\,dk, \tag{83}$$

where $\Gamma_k = 1/T_k$ and the value $\beta I(p) = 3\times 10^{-2}$ was used in (78), which is consistent with values considered by Phillips (1985) for $p = \frac{1}{2}$ and with the observational estimates $\beta \approx 0.012$ and $I(p) \approx 2.5$ (Juszko et al. 1995; Thomson et al. 2013) . Recent observations tend to suggest larger values of p, such as $p = 1$ or $p = 2$, but these will generally imply smaller values of $\beta I(p)$ and a smaller wave-drift component, so the smaller value of p and larger value of $\beta I(p)$ are retained here. The total pressure forcing F_{w0} on the wave field is the vertical integral of $F_w(z)$,

$$F_{w0} = \int_{-\infty}^{0} F_w(z)\,dz, \tag{84}$$

and the fraction b_0 of wind-stress deposited into the wave-field by the wave-correlated pressure forcing is

$$b_0 = \frac{F_{w0}}{\tau_0}. \tag{85}$$

For physical consistency, it is necessary to require $b_0 < 1$. This requirement was enforced by imposing an ad-hoc linear dependence of the high-wavenumber integration limit on the 10-m wind speed,

$$k_1 = 0.15 \times U_{10N} \quad \text{for units} \quad [k_1, U_{10N}] = [\mathrm{m}^{-1}, \mathrm{m\ s}^{-1}]. \tag{86}$$

This results in a value of b_0 that is roughly proportional to U_{10N}, with $b_0 \approx 0.8$ at $U_{10N} = 20$ m s^{-1} (Fig. 5).

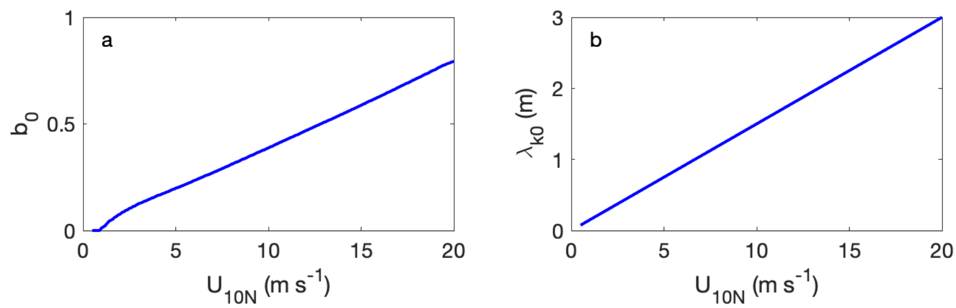

FIG. 5. (a) Wave-forcing wind-stress fraction b_0 and (b) spectral integral short-wave limit $\lambda_{k0} = 2\pi/k_0$ vs. 10-m wind speed for the wave-drift solutions used for the combined wind-drift and wave-drift model solutions.

The corresponding profile of wave-breaking drag from the rotating equilibrium-sea wave-drift equations (69) was computed as the spectral integral

$$\tau_{br}(z) = -\int_{k_0}^{k_1} \Gamma_k \hat{\mathbf{U}}_S(z;k)\, k\, dk = -\int_{k_0}^{k_1} \frac{1}{T_k} \hat{\mathbf{U}}_S(z;k)\, k\, dk, \tag{87}$$

where in (79), the value $\beta I(p) = 3\times 10^{-2}$ was again used. For simplicity, the nonlinear spectral momentum fluxes into and within the equilibrium range were neglected. To conserve momentum in the combined wave-drift and wind-drift system, the rate of momentum gained by the mean drift must then be equal to that lost from the wave field by breaking, so that the effective body force in the mean wind-drift equations $\mathbf{F}_{br}$ is equal and opposite to τ_{br},

$$\mathbf{F}_{br}(z) = -\tau_{br}(z). \tag{88}$$

As solved here, the resulting model equations of Samelson (2022) for the mean wind-drift $\mathbf{U} = (U, V)$, modified to include the forcing $\mathbf{F}_{br} = (F_{br}^x, F_{br}^y)$ from the parameterized wave-breaking drag, take the form

$$-fV = \frac{d}{dz}\left[\phi_w \kappa u_* (z_0 - z)\frac{dU}{dz}\right] + F_{br}^x(z), \tag{89}$$

$$fU = \frac{d}{dz}\left[\phi_w \kappa u_* (z_0 - z)\frac{dV}{dz}\right] + F_{br}^y(z). \tag{90}$$

Here the wave-correction factor ϕ_w and effective roughness length z_0 are functions of U_{10N} as specified by Samelson (2022), κ is the von Kàrmàn constant, and $u_* = (\tau_0/\rho_0)^{1/2}$ is the water friction velocity. The uniform proportionality of the eddy viscosity in (89)-(90) to $z_0 - z$ simplifies the solution of (89)-(90), relative to the piecewise-continuous eddy viscosity from Samelson (2022), with minimal effect on the solution structure for the cases considered here.

With the definitions

$$W = U + iV, \quad W_F = \frac{1}{f}(F^y_{br} - iF^x_{br}), \quad \xi = (1+i)\left[\frac{2f}{\phi_w \kappa u_*}(z_0 - z)\right]^{1/2}, \tag{91}$$

the equations (89)-(90) may be rewritten as

$$\frac{d^2W}{d\xi^2} + \frac{1}{\xi}\frac{dW}{d\xi} - W = -W_F, \tag{92}$$

and solved in terms of the modified Bessel functions $K_0(\xi)$ and $I_0(\xi)$, as shown for the homogeneous case ($W_F = 0$) by Ellison (1956) and described in the appendix of Samelson (2022). A particular solution W_p,

$$W_p(\xi) = A_p(\xi)\,K_0(\xi) + B_p(\xi)\,I_0(\xi), \tag{93}$$

$$A_p(\xi) = \int_{\xi_\infty}^{\xi} \xi'\, I_0(\xi')\, W_F(\xi')\, d\xi', \tag{94}$$

$$B_p(\xi) = -\int_{\xi_\infty}^{\xi} \xi'\, K_0(\xi')\, W_F(\xi')\, d\xi', \tag{95}$$

where ξ_∞ denotes the limit $\xi(z \to -\infty)$, may be obtained by variation of parameters.

The full solution W, which consists of the sum of the particular solution W_p and a homogeneous solution W_h, must satisfy $W \to 0$ as $z \to -\infty$ and the surface stress condition,

$$-\phi_w \kappa u_* z_0 \left.\frac{dW}{dz}\right|_{z=0} = -(1-b_0)u_*^2, \tag{96}$$

where $1 - b_0$ is the fraction of downward wind stress $\tau_0 = \rho_0 u_*^2$ transferred directly to the mean wind-drift. The first of these boundary conditions requires that $W_h = A_h K_0$ and the second then determines A_h:

$$A_h = (1-b_0)A - A_p(\xi_0) + B_p(\xi_0)\,\frac{I_1(\xi_0)}{K_1(\xi_0)}, \tag{97}$$

where

$$A = \left(\frac{u_*^3}{f\phi_w\kappa z_0}\right)^{1/2} \frac{e^{-i\frac{\pi}{4}}}{K_1(\xi_0)} \tag{98}$$

and

$$\xi_0 = \xi|_{z=0} = (1+i)\left(\frac{2fz_0}{\phi_w\kappa u_*}\right)^{1/2}, \tag{99}$$

as in equations (A2) and (A3) of the appendix of Samelson (2022). The full solution of the wave-forced wind-drift model is then

$$W(\xi) = U(\xi) + iV(\xi) = [A_h + A_p(\xi)]\,K_0(\xi) + B_p(\xi)\,I_0(\xi), \tag{100}$$

which can be written in vector form and as a function of depth z as

$$\mathbf{W}(z) = [U(z), V(z)], \quad U(z) = \mathrm{Re}\{W[\xi(z)]\}, \quad V(z) = \mathrm{Im}\{W[\xi(z)]\}, \tag{101}$$

where Re$\{\cdot\}$ and Im$\{\cdot\}$ denote the real and imaginary parts, respectively.

The total combined mean equilibrium-sea wind-drift and wave-drift vector $\mathbf{U}_m$ is the sum of the vector wind-drift $\mathbf{W}$ from (101) and the spectral-integral vector wave-drift $\mathbf{U}_S$ from (80):

$$\mathbf{U}_m(z) = \mathbf{W}(z) + \mathbf{U}_S(z). \tag{102}$$

Relative to the wind-drift-only solution obtained by setting $b_0 = A_p = B_p = 0$ in (97) and (100), which is essentially equivalent at a given U_{10N} to the corresponding solution obtained by Samelson (2022), the wave forcing and drift cause modest but systematic changes to the total mean drift profile (Figs. 6,7). The main changes are an increase in near-surface shear and a decrease in the cross-wind component of drift for the total mean drift relative to the wind-drift-only solutions. These differences increase with wind speed. The near-surface shear difference is dependent on the particular choice of parameterizations $\phi_w(U_{10N})$ and $z_0(U_{10N})$ for the wind-drift model. The pressure-forcing fractions b_0 of total wind stress for these solutions were $b_0 = 0.27$ for $U_{10N} = 7$ m s^{-1} (Fig. 6) and $b_0 = 0.63$ for $U_{10N} = 16$ m s^{-1} (Fig. 7).

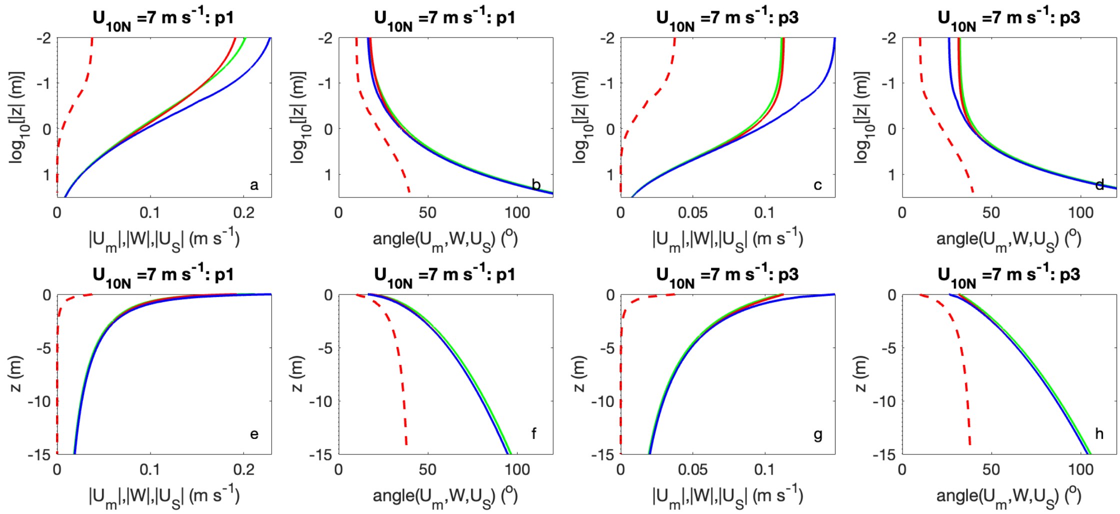

FIG. 6. Profiles of (a,c,e,g) magnitude and (b,d,f,h) clockwise wind-relative angle of total wind and wave drift $\mathbf{U}_m$ from (102) (blue lines) and corresponding wind-drift-only (green) profiles vs. (a-d) 10-based logarithm of depth z (m) and (e-h) depth z (m) for $U_{10N} = 7$ m s^{-1} and Coriolis parameter f computed at 40° N. The profiles are shown for two different parameterizations of the wind-drift model wave-correction factor $\phi_w(U_{10N})$ and roughness length $z_0(U_{10N})$: "p1" (a,b,e,f) is the "monochromatic" parameterization described by Samelson (2022) and "p3" (c,d,g,h) is the adjusted version of p1 described by Leyba et al. (In preparation). The wave-drift $\mathbf{U}_S$ (dashed red) and wave-forced wind-drift $\mathbf{W}$ (solid red) components of $\mathbf{U}_m$ from (102) are also shown.

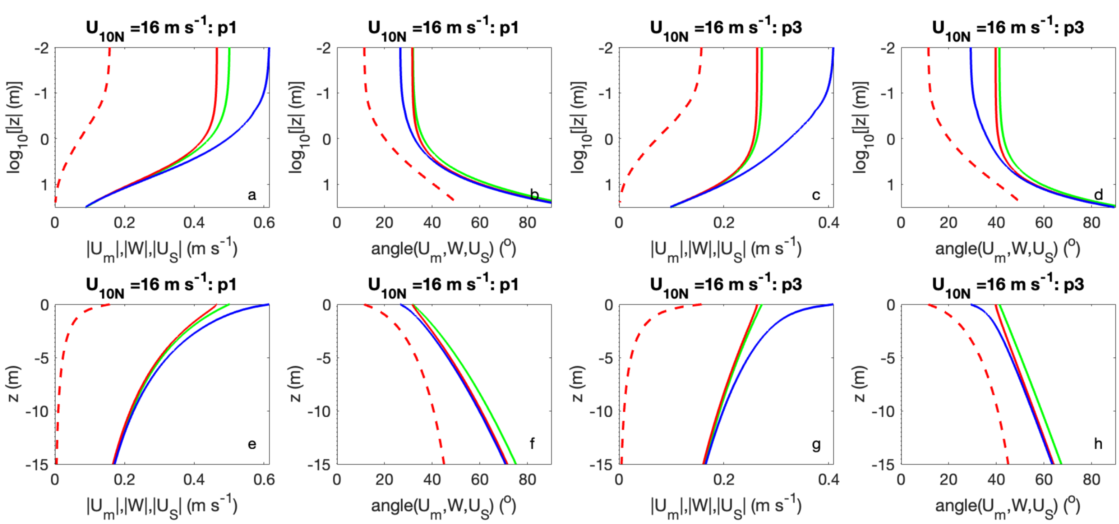

FIG. 7. As in Fig. 6 but for $U_{10N} = 16$ m s^{-1}.

6. Stokes drift budget for wave-averaged Langmuir circulation modeling

The steady rotating wave-drift equations (69) can be extended to a time-dependent system in a straightforward, if ad-hoc, way by restoring the time rates of change $(dU_S/dt, dV_S/dt)$ in the mean-drift momentum balance. The resulting time-dependent horizontal momentum equations for the surface-conforming mean wave drift in the rotating case are:

$$\frac{dU_S}{dt} - fV_S = \overline{-\frac{1}{\rho_0}\frac{\partial p'_p}{\partial x}} - \Gamma_S U_S = -\Gamma_S(U_S - \overline{u}_p), \tag{103}$$

$$\frac{dV_S}{dt} + fU_S = -\Gamma_S V_S, \tag{104}$$

where from (51), (55), and (62),

$$\overline{u}_p = \sigma k a_p^2 e^{2kz}. \tag{105}$$

This approach implicitly assumes that the wind forcing changes slowly relative to the equilibrium-sea timescales T_S and T_k, which are typically on the order of a few hours or less, except at the longer wavelengths for strong wind forcing.

As in the steady case, the damping coefficient Γ_S in (103)-(104) and the equilibrium-sea wave parameters σ, k, and a_p in (105), which determine the momentum forcing in (103), may be viewed or specified either monochromatically, for a single wave representing the equilibrium conditions, or spectrally, as a function of wavenumber in the equlibrium range. In the monochromatic case, with a_p as in (58) with $\Gamma_S = \beta_k$, (105) can be written

$$\overline{u}_p = \left(\frac{2kb_0\tau_0}{\rho_0\beta_k}\right) e^{2kz}. \tag{106}$$

In the spectral case, $\overline{u}_p$ will take a spectral density form as in (78), and the resulting solution $\hat{\mathbf{U}}_S(t; z, k)$ of (103)-(104) will represent a spectral density that must be integrated over the equilibrium range to obtain the vector mean drift, as in (80).

In either case, the result of this extension is a time-dependent momentum budget for the Stokes drift. In principle, this budget could be used in conjunction with the standard wave-averaged Boussinesq system to model, for example, Langmuir circulation dynamics under equilibrium-sea conditions with slowly varying wind forcing. Such a budget equation has not been previously available; instead, a time-dependent Stokes-drift forcing has typically been inserted into the wave-averaged system without regard to the associated momentum conservation balances. In this setting, it seems likely that it may again be appropriate to apportion the wind stress forcing between the mean drift and wave-averaged equations and then to include the wave-drift damping term again as a body force in the wave-averaged equations.

A more rigorous approach may be possible through a Helmholtz-like decomposition of the velocity field, in which the wave velocity field is represented as a potential flow in the downwind-vertical plane plus a cross-wind component of higher order that can be written as a functional $V[\phi]$ of the downwind-vertical potential $\phi(x,z)$ and the turbulent component is written in terms of a vector potential $\mathbf{H} = (H^x, H^y, H^z)$:

$$\mathbf{u} = (u,v,w) = \left(\frac{\partial \phi}{\partial x}, V[\phi], \frac{\partial \phi}{\partial z}\right) + \left(\frac{\partial H^z}{\partial y} - \frac{\partial H^y}{\partial z}, \frac{\partial H^x}{\partial z} - \frac{\partial H^z}{\partial x}, \frac{\partial H^y}{\partial x} - \frac{\partial H^x}{\partial y}\right). \tag{107}$$

Following the outline of the explicit linear solution in Sections 2 and 3, the linear potential-flow wave solution and associated second-order wave drift balance would be developed from the divergence of the momentum balance in the downwind-vertical plane. From (2), the functional $V[\phi]$ should take the form

$$V[\phi] = e^{-\Gamma s t} \int^t e^{\Gamma s t'} \frac{\partial \phi}{\partial x} \, dt', \tag{108}$$

where the separation of the wave-coherent component $V[\phi]$ from the turbulent cross-wind velocity may be motivated by ensemble averaging for random fields or other similar arguments. The curl of the three-dimensional momentum balance should yield equations for the turbulent component that can be averaged over the wave timescale, with the usual wave-averaging assumptions, to obtain the vortex-force or equivalent wave-turbulent interactions terms that drive Langmuir circulations.

Such an approach seems plausible but is beyond the scope of the present study, the main goal of which was to extend the semi-empirical, equilibrium-sea wind-drift model of Samelson (2022) to include explicit representation of the wave-drift component, as described in Section 5. In that extended semi-empirical model, all turbulent dynamics including any Langmuir wave-turbulence interaction components are represented only in mean, implicit, parameterized form, through the depth-dependent eddy viscosity terms in (89)-(90).

7. Summary

The simple physical representation of wave-breaking dissipation assumed in this work provides qualitative insight into the potential effect of the Earth's rotation on near-surface wave-drift. The associated forced-damped solutions suggest that the mean equilibrium-sea wave-drift will be rotated away from the downwind direction in the Ekman-rotation sense, with larger rotation for the longer-wavelength drift components that extend to greater depths and less rotation for the shorter-wavelength components that are trapped closer to the surface. This perhaps surprising result can be understood as a damped-wave modification of the Hasselmann (1970) near-inertial component of the inviscid rotating-wave drift dynamics, in which the Hasselmann (1970) homogeneous-solution inertial balance is replaced by a steady rotation that is controlled by the damping timescale.

The rotating equilibrium-sea wave and wind drift model constructed by combining the rotating wave-drift model and the Samelson (2022) wind-drift model, with the wind-drift model supplemented by the implied flux of momentum from the wave field into the mean flow, gives a modified picture of the total wave and wind drift under equilibrium conditions. In the combined model, the predicted rotation from downwind of the total subsurface drift is again in the Ekman sense but is reduced from that predicted by the wind-drift model alone. These results primarily rely on basic physical balances and simple but arguably plausible assumptions regarding the qualitative and, in part, quantitative characteristics of the rotating equilibrium-sea dynamics. Among the important uncertainties are the extent to which the linear wave-damping is representative of the momentum-flux processes associated with wave dissipation and breaking and the extent to which the wave and mean drift dynamics can be separately modeled and then combined, as is assumed for the combined wave and wind drift model.

An alternative hypothesis regarding the momentum distribution from surface wave-breaking is that it is deposited at or very close to the surface (e.g., Craig and Banner 1994; Sullivan et al. 2004). If the wave-breaking momentum is deposited into the mean flow at the surface, then all the wind momentum is effectively transferred to the mean flow at the surface in the equilibrium-sea regime, because the mean momentum transport into the wave field must be equal to the transport out of the wave field and into the mean flow. In that case, the momentum distribution from surface wave-breaking is effectively represented in the equilibrium-sea wind-drift model as formulated by Samelson (2022), which is driven at the surface by the full wind stress and does not include any subsurface forcing that might be associated with wave-dynamical processes. From this point of view, the explicit wave-drift model presented here and the wind-drift model as formulated by Samelson (2022) can be interpreted as two extreme members of a range of hypotheses regarding the vertical distribution of the momentum deposition from surface wave-breaking. The linear drag considered here then represents the assumption of subsurface deposition over the full depth extent of the mean wave drift. Note that in the numerical experiments of Sullivan et al. (2004), the wave-breaking momentum deposited at or very close to the surface was rapidly mixed vertically, suggesting a qualititative consistency with the linear-damping body-force representation even in that case.

The question of separability of mean wave and wind drift dynamics is relevant also for the extension of these ideas to models of wave-turbulence interaction, including the formulation of wave-averaged equations for the modeling of Langmuir circulations. An additional and perhaps more fundamental uncertainty is the extent to which linear theory accurately captures near-surface ocean wave drift, with or without rotation, as direct measurements of wave drift that might show agreement with or departure from kinematic predictions of Stokes drift based on observed surface-wave conditions are generally not available. Work in progress that will be described elsewhere (Leyba et al. In preparation) has demonstrated significant skill of the Samelson (2022) wind-drift model, based on comparisons with an extensive surface-velocity dataset from a recent observational program (Farrar et al. 2025), which provides support for some of the basic ideas and model formulations that provide the context for the present study. Further work on these and related topics is merited and should help to clarify the physical basis and implications of these suggestive results.

Acknowledgments. This research was supported for RMS by the National Aeronautics and Space Administration (NASA) Ocean Vector Winds Science Team (NASA Grant No. 80NSSC23K0986) and the NASA Earth Venture Suborbital-3 program (NASA Grant No. 80NSSC19K1011) and by the Office of Naval Research (ONR Grant No. N00014-23-1-2579), and for SFZ by the National Science Foundation (NSF Grant Nos. 2023020 and 2316818), the NASA Salinity and Stratification at the Sea Ice Edge (SASSIE) project (NASA Grant No. 80NSSC21K0832), and the Department of Energy Wind Forecast Improvement Project-3 (DOE Grant No. DE-EE0009424). Conversations with E. D. Skyllingstad are gratefully acknowledged.

Data availability statement. Code used for the calculations and figures in this study has been archived at https://github.com/rsamelson/SDWDRES and will be made publicly accessible upon publication.

References

Ardhuin, F., L. Marié, N. Rascle, P. Forget, and A. Roland, 2009: Observation and estimation of Lagrangian, Stokes, and Eulerian currents induced by wind and waves at the sea surface. *Journal of Physical Oceanography*, **39 (11)**, 2820–2838.

Ardhuin, F., and Coauthors, 2010: Semiempirical dissipation source functions for ocean waves. Part I: Definition, calibration, and validation. *Journal of Physical Oceanography*, **40 (9)**, 1917 – 1941.

Breivik, Ø., P. A. E. M. Janssen, and J.-R. Bidlot, 2014: Approximate Stokes drift profiles in deep water. *Journal of Physical Oceanography*, **44 (9)**, 2433 – 2445.

Buckley, M. P., F. Veron, and K. Yousefi, 2020: Surface viscous stress over wind-driven waves with intermittent airflow separation. *Journal of Fluid Mechanics*, **905**, A31.

Chereskin, T. K., 1995: Direct evidence for an Ekman balance in the California Current. *Journal of Geophysical Research*, **100**, 18 261–18 269.

Craig, P. D., and M. L. Banner, 1994: Modeling wave-enhanced turbulence in the ocean surface layer. *J. Phys. Oceanogr.*, **24**, 2546–2559.

D'Asaro, E. A., J. Thomson, A. Y. Shcherbina, R. R. Harcourt, M. F. Cronin, M. A. Hemer, and B. Fox-Kemper, 2014: Quantifying upper ocean turbulence driven by surface waves. *Geophysical Research Letters*, **41 (1)**, 102–107.

Ekman, V. W., 1905: On the influence of the Earth's rotation on ocean currents. *Arkiv Mat. Astronom. Fyzik*, **2**, 1–53.

Ellison, T. H., 1956: Atmospheric turbulence. *Surveys in Mechanics*, G. K. Batchelor, and R. M. Davies, Eds., Cambridge University Press, 400–430.

Farrar, J. T., and Coauthors, 2025: S-MODE: the Sub-Mesoscale Ocean Dynamics Experiment. *Bulletin of the American Meteorological Society*.

Grare, L., L. Lenain, and W. K. Melville, 2018: Vertical profiles of the wave-induced airflow above ocean surface waves. *Journal of Physical Oceanography*, **48 (12)**, 2901–2922.

Hasselmann, K., 1970: Wave-driven inertial oscillations. *Geophysical Fluid Dynamics*, **1 (3-4)**, 463–502.

Juszko, B.-A., R. F. Marsden, and S. R. Waddell, 1995: Wind stress from wave slopes using phillips equilibrium theory. *Journal of Physical Oceanography*, **25 (2)**, 185 – 203.

Komen, G. J., L. Cavaleri, M. Donelan, K. Hasselmann, S. Hasselmann, and P. A. E. M. Janssen, 1994: *Dynamics and Modelling of Ocean Waves*. Cambridge University Press.

Laxague, N. J. M., and C. J. Zappa, 2020: Observations of mean and wave orbital flows in the ocean's upper centimetres. *Journal of Fluid Mechanics*, **887**, A10.

Leyba, I. M., R. M. Samelson, J. T. Farrar, L. Grare, L. Lenain, C. B. Rocha, and E. Rodríguez, In preparation: Calibration of a wind-drift model using remote-sensing and in-situ near-surface velocity observations.

Morey, S. L., N. Wienders, D. S. Dukhovskoy, and M. A. Bourassa, 2018: Measurement characteristics of near-surface currents from ultra-thin drifters, drogued drifters, and HF radar. *Remote Sensing*, **10 (10)**, 1633.

Phillips, O. M., 1958: The equilibrium range in the spectrum of wind-generated ocean waves. *J. Fluid Mech.*, **4**, 426–434.

Phillips, O. M., 1977: *The Dynamics of the Upper Ocean*. 2nd ed., Cambridge University Press.

Phillips, O. M., 1985: Spectral and statistical properties of the equilibrium range in wind-generated gravity waves. *Journal of Fluid Mechanics*, **156**, 505–531.

Pizzo, N., L. Deike, and A. Ayet, 2021: How does the wind generate waves? *Physics Today*, **74 (11)**, 38–43.

Pizzo, N., and G. L. Wagner, 2025: Deep flows transmitted by forced surface gravity waves. *Water Waves*, **7**, 389–406.

Plant, W. J., 1982: A relationship between wind stress and wave slope. *J. Geophys. Res.*, **87**, 1961–1967.

Rascle, N., and F. Ardhuin, 2009: Drift and mixing under the ocean surface revisited: Stratified conditions and model-data comparisons. *Journal of Geophysical Research: Oceans*, **114 (C2)**.

Resio, D. T., V. R. Swail, R. E. Jensen, and V. J. Cardone, 1999: Wind speed scaling in fully developed seas. *Journal of Physical Oceanography*, **29 (8)**, 1801 – 1811.

Samelson, R. M., 2022: Wind drift in a homogeneous equilibrium sea. *J. Phys. Oceanogr.*, **52**, 1945–1967.

Sullivan, P. P., and J. C. McWilliams, 2010: Dynamics of winds and currents coupled to surface waves. *Annual Review of Fluid Mechanics*, **42 (1)**, 19–42

Sullivan, P. P., J. C. McWilliams, and W. K. Melville, 2004: The oceanic boundary layer driven by wave breaking with stochastic variability. Part 1. direct numerical simulations. *Journal of Fluid Mechanics*, **507**, 143–174.

Sutherland, P., and W. K. Melville, 2015: Field measurements of surface and near-surface turbulence in the presence of breaking waves. *Journal of Physical Oceanography*, **45 (4)**, 943 – 965.

Thomson, J., E. A. D'Asaro, M. F. Cronin, W. E. Rogers, R. R. Harcourt, and A. Shcherbina, 2013: Waves and the equilibrium range at ocean weather station p. *Journal of Geophysical Research: Oceans*, **118 (11)**, 5951–5962.

van den Bremer, T. S., and Ø. Breivik, 2018: Stokes drift. *Philosophical Transactions of the Royal Society A: Mathematical, Physical and Engineering Sciences*, **376 (2111)**, 20170 104.

Xu, Z., and A. J. Bowen, 1994: Wave- and wind-driven flow in water of finite depth. *J. Phys. Oceanogr.*, **24**, 1850–1866.

Zelenke, B., C. O'Connor, C. Barker, and C. Beegle-Krause, 2012: General NOAA Operational Modeling Environment (GNOME) technical documentation. Tech. Rep. Technical Memorandum NOS OR OR&R 41, National Oceanic and Atmospheric Administration, Office of Response and Restoration: Seattle, WA, USA.